Chapter 2: Experimental techniques for the characterization of lyotropic liquid crystalline phases

Mukesh Chandra Bos and Santosh Prasad Gupta

Mukesh Chandra Bos: Affiliations- B. N. College, Patna University, Patna and Department of Physics, Patna University, Patna – 800005. Email- drmukeshchandrabosphybnc@pup.ac.in

Santosh Prasad Gupta: Affiliation- Department of Physics, Patna University, Patna – 800005. Email-santosh-phy@patnauniversity.ac.in

A brief overview of the experimental methods used to characterize lyotropic liquid crystalline phases is provided in this chapter. A combination of amphiphiles (such as surfactants) and solvents (such as water) can generate lyotropic liquid crystals. As a result, at certain concentrations, pressures, and temperatures, these phases are thermodynamically stable. Similar to thermotropics, there are several architecturally different variations that are referred to as lyotropic liquid crystals.

A basic overview of the X-ray diffraction (XRD) method is provided in Section 2.1. This method is a flexible non-destructive analytical approach that may be used to examine the phase composition, crystal structure, and orientation of materials that are solid, powder or liquid. A basic introduction to polarizing optical microscopy (POM) is provided in section 2.2. In section 2.3, the specific characterization of the different lyotropic phases is covered in relation to the XRD and POM techniques.

2.1: X-ray diffraction technique

X-Ray diffraction analysis (XRD) is a nondestructive technique that provides detailed information about the crystallographic structure, chemical composition, and physical properties of a material. It is based on the constructive interference of monochromatic X-rays and a crystalline sample. X-rays are shorter wavelength electromagnetic radiation that are generated when electrically charged particles with sufficient energy are decelerated. In XRD, the generated X-rays are collimated and directed to a nanomaterial sample, where the interaction of the incident rays with the sample produces a diffracted ray, which is then detected, processed, and counted. The intensity of the diffracted rays scattered at different angles of material are plotted to display a diffraction pattern.

Each phase of the material produces a unique diffraction pattern due to the material's specific chemistry and atomic arrangement. The diffraction pattern is a simple sum of diffraction patterns

of each phase. Imperfection in the sample material would affect the pattern of the diffracted signal. In this case, the factors that contribute to the imperfection of the sample would be the composition heterogeneity, crystal structure defects, microstains, and crystallite size.

2.1.1: Theory of X-ray diffraction

X-rays are transverse electromagnetic radiation with wave length in the range (~0.01-10nm), lying between ultraviolet (UV) and gamma radiation. They are scattered by the electrons in the irradiated material. Therefore, the intensity of scattered radiation depends upon the electron density distribution in the material. The interference of x-rays scattered by different electrons gives rise to the observed diffraction pattern [1]. Therefore, we consider only coherent, elastic scattering events.

Let us consider a monochromatic planar wave incident on a point scatterer, such as an electron, sitting at the origin. It can be written as, [2].

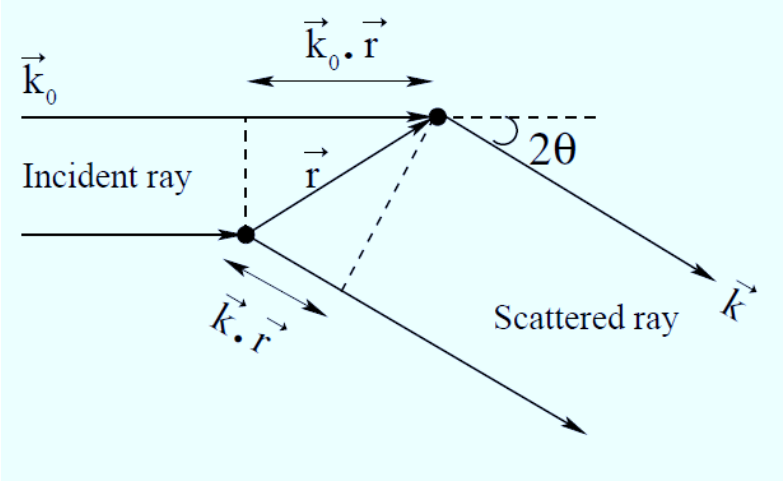

Fig. 2.1: Geometric arrangement of scattering event from two scattering centers separated by a distance r.

$$\Phi_{in} = \Phi_o \, e^{ik_o r}$$

where Φ_o is the amplitude of the plane wave with wave vector k_o. The amplitude of the scattered spherical wave at a distance R can be written as,

$$\Phi_{sc} = \frac{\Phi_o \, a}{R} e^{ikR}$$

where a is the 'scattering length', which determines the strength of scattering. Now consider another electron at a distance r from the first one (Fig. 2.1). The phase difference between the rays scattered by the two electrons can be expressed as $(k - k_o).r$ where k is the wave vector in the direction of scattering. $q = k - k_o$ is known as the scattering vector and its magnitude is given by $|q| = (4\pi\sin\theta)/\lambda$, where 2θ is the scattering angle between k and k_o. The amplitude of the scattered

wave at R (>> r) where the scattered rays can be treated as parallel is given by,

$$\Phi_{sc} = \frac{\Phi_o\, a}{R} e^{i(kR-qr)}$$

For an assembly of N scatterers at r_n (n= 1, 2, 3, . . . N), the above expression can be summed up to get the total amplitude of the scattered beam.

$$\Phi_{tot} = \frac{\Phi_o\, a}{R} e^{ikR} \sum_{r_n} e^{i(-qr_n)}$$

For a material of electron density

$$\rho(r) = \sum_{r_n} \delta(r - r_n)$$

the above equation can be modified to

$$\Phi_{tot} = \frac{\Phi_o\, a}{R} e^{ikR} \int e^{i(-qr)}\, dr$$

This expression shows that the amplitude of the scattered wave is proportional to the Fourier transform of the electron density function of the scattering medium. The expression is derived based on the assumption that multiple scattering from the medium is negligible. The intensity of scattered radiation is the square of its amplitude and hence is given by,

$$I(q) = |\Phi_{tot}|^2 = |\frac{\Phi_o\, a}{R} e^{ikR} \int e^{i(-qr)}\, dr|^2$$

In the following chapters of this thesis x-ray diffraction technique has been used to identify various lyotropic liquid crystalline phases. For such periodic structures, the electron density *ρ(r)* can be written as the convolution of a lattice function $\rho_l(r)$, describing the periodic lattice and a basis function $\rho_b(r)$, describing the electron density within each unit cell.

$$\rho(r) = \rho_l(r) \otimes \rho_b(r)$$

Since the Fourier transform of the convolution of two functions is the product of their Fourier transforms from above equation, we get,

$$\int \rho(r) e^{i(-qr)}\, dr = \int \rho_l(r) e^{i(-qr)}\, dr \int \rho_b(r) e^{i(-qr)}\, dr = F_l\, F_b$$

where $F_l(q)$ and $F_b(q)$ are the Fourier transforms of the lattice and basis functions, respectively. Now, the scattered intensity can be expressed as,

$$I(q) \sim |F_l(q)|^2\, |F_b(q)|^2 = S(q)\, P(q)$$

Here $S(q) = |F_l(q)|^2$, called the 'structure factor', determines the points in the reciprocal lattice, and $P(q) = |F_b(q)|^2$ the 'form factor' determines the intensity at these points. For an infinite 3-

D lattice defined by the crystallographic unit vectors ***a***, ***b*** and ***c*** the lattice function will be a 3D array of δ functions, given by [54],

$$\rho(r) = \sum_{m,n,p} \delta(r - (m\,a + n\,b\ + p\,c))$$

where m, n and p are integers. The Fourier transform of this function is,

$$F_l\,(q) = \sum_{h,k,l} \delta(q - (h\,a^* + k\,b^* + l\,c^*))$$

where a∗, b∗ and c∗ are the basis vectors in the reciprocal lattice and h, k and l are integers. Finally, the scattered intensity can be written as,

$$I(q) \sim \frac{|F_b\,(q)|^2}{(a.\,(b\ x\ c))^2}\ |\sum_{h,k,l} \delta(q - (h\,a^* + k\,b^* + l\,c^*))\,|^2$$

From this expression, it can again be seen that the diffraction pattern of an infinite lattice is another infinite 3D lattice. The position of the diffraction peaks is determined by the Miller indices (hkl) and their intensities by the value of the form factor at these reciprocal lattice points.

2.1.2: Polarization, Geometric and Multiplicity corrections to the Intensity

The scattered intensity from a sample is affected by certain factors that depend on the scattered angle, nature of the sample and the type of the detector used for the experiment. Therefore, the observed intensities have to be corrected for these effects before they can be put on a relative scale. The corrected scattered intensity is given by,

$$I\,(q) = A\,P(q)\,g(q)\,I_o(q)$$

where A is an independent scale factor, p is the polarization factor, g is the geometric factor and I_o is the observed intensity. The polarization factor,

$$p = \frac{1}{1 + Cos^2(2\Theta)}$$

and arises from the fact that the incident x-ray beam is unpolarized while scattered x-ray beam is polarized [3]. $Cos(2\Theta) \sim 1$ in the small angle region and hence, this correction can be ignored for small angle scattering.

The geometric factor depends both on the type of the sample and geometry of the detector used to record the data. In case of unoriented samples, the scattered intensities corresponding to each peak is distributed over a spherical shell of radius q. If the detector used to collect the data, is one dimensional (1D) such as a position sensitive detector (PSD), then the observed intensity has to be multiplied by a factor $4\pi q^2$; the area of the shell, in-order to get the total intensity, because 1D

detector intersect the spherical shell at two points. On the other hand, a 2D detector, such as image plate, cuts the spherical shell along a plane, resulting in a ring. If the observed intensities are integrated over these then they have to further multiplied by q to get the total intensity. In-order to construct the electron density map from the diffraction data, intensities of the peaks corresponding to the different lattice planes have to be calculated, this requires an additional correction factor called the multiplicity factor along with the above-mentioned intensity corrections. In the case of unoriented samples, reflections from equivalent lattice planes can overlap, at the same value of q in the diffraction pattern. The observed intensity has to be scaled (divided) by a multiplicity factor to get the intensity of any one of the overlapping peaks, corresponding to a particular lattice plane. The multiplicities are lower in lower symmetry systems and very high in highly disordered systems. For example, the peaks corresponding to the lattice planes (100), (010), (001), $(\bar{1}00)$, $(0\bar{1}0)$ and $(00\bar{1})$, from a cubic lattice overlap in the diffraction pattern of unoriented samples. Therefore, we have to divide the intensity by 6 to obtain the intensity of the (100) peak.

2.1.3: Experimental setup

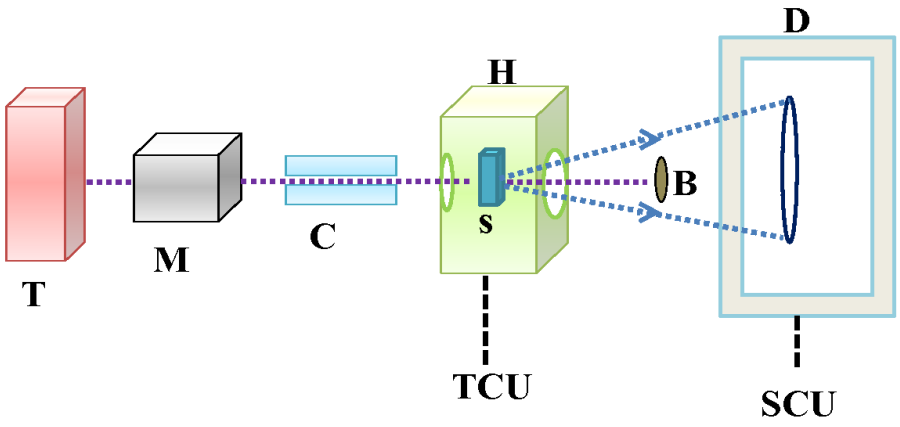

Fig. 2.2: Schematic of the experimental set up used for x-ray diffraction study. T, M, C, H, B, S, D, TCU and SCU denotes the x-ray generator, monochromator, collimator, the heater, beam-stop, sample, detector (imageplate), temperature control unit, and the scanning control unit respectively. The dashed violet and blue lines represent the incident and scattered rays respectively.

In figure 2.2, the experimental setup for x-ray diffraction experiments is displayed. Anode x-ray generators or shield tube units running at 50 kV and 80 mA are commonly utilised to create X-rays. Utilizing a multilayer focusing mirror is the standard method for selecting CuKα radiation with a wavelength of 0.154 nm. In a temperature-controlled heater with a stability of 0.1 K, the

liquid sample is utilised to fill a glass capillary (Hampton Research, outer diameter 0.5 to 1 mm, wall thickness 0.01 mm). Usually, an image plate is used to gather the information. Normally, there is a 200–350 mm range for the sample to detector distance. One hour to thirty minutes is the usual exposure duration.

2.2 Polarizing optical microscopy (POM)

Polarizing optical microscopy is widely used to identify different liquid crystalline phases [4]. Liquid crystalline phases are birefringent and show characteristic textures between crossed polarizers under an optical microscope, which arise due to the defects in the medium. These defects create deformations in the medium over length scales of the order of tens of micrometers due to the low elastic constants of the system. Since, the type of defect in the medium is determined by the symmetry of the structure, the textures resulting from these defects are characteristic of the phase. Therefore, these textures can be used as fingerprints to identify different liquid crystalline phases as discussed in the last section.

As an example, we shall briefly discuss the defects and corresponding texture in a nematic liquid crystal. Nematic phase is characterized by long range orientational order and short-range positional order. Orientational ordering in the medium is described in terms of an apolar unit vector, called the director ($\vec{n}$).

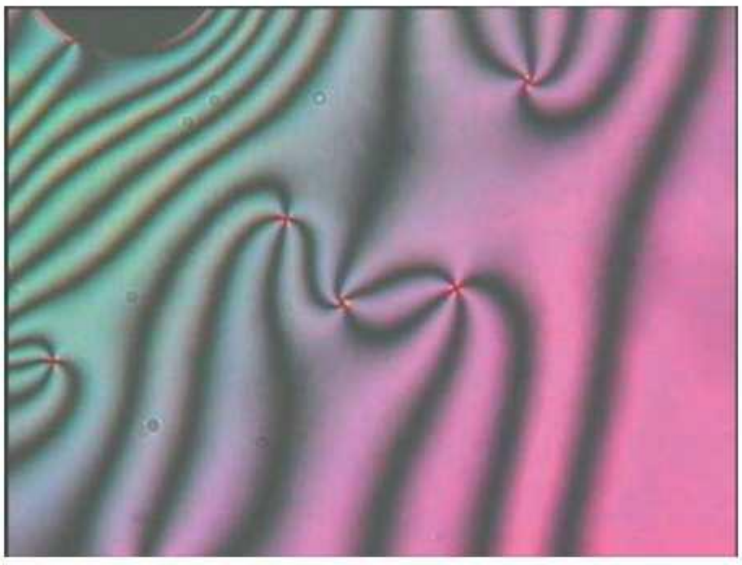

Fig. 2.3: Typical Schlieren texture of nematic phase (from ref. [9]).

Nematics between untreated glass plates often orient with their director parallel to the substrates. If this orientation is not homogeneous, but varies slowly in the plane of the substrate, so-called Schlieren textures [5–7] are observed between crossed polarizers (Fig. 2.3). Schlieren textures

exhibit characteristic sets of often curved dark brushes. These correspond to the extinction position of the nematic director field, with $n(\vec{r})$ coinciding with the direction of either the polarizer or the analyzer. A closer look reveals that the brushes come together in a singular point and can be two-fold or four-fold [8]. The singularities are topological defects, called disclinations, which are assigned a certain strength **s**. The absolute value of the strength of the disclination is obtained by dividing by four the number of brushes cutting a 2π circle around the center, i.e. $|\mathbf{s}|$= number of brushes/4. The sign of the defect strength can be obtained by rotation of the polarizers: the defect is assigned a plus (+) sign if the dark brushes rotate in the same direction as the polarizers and a minus (-) sign if they rotate in the opposite direction. Note that in any case the point singularities do not move and the rotation of the brushes is continuous, due to a continuous variation of the director field $n(\vec{r})$. Experimentally, only s = ±1/2 and s = ±1 defects are observed for nematic liquid crystals. Two-fold and four-fold singularities, also of different sign, generally occur simultaneously in the same sample. The corresponding director configurations are schematically shown in figure 2.4, as a top view on the substrate plane. If the disclination lines make a large angle with the direction of observation they give rise to the 'threaded' texture. These disclination lines either form closed loops in the medium or end at the surfaces. In fact, these thread-like structures are responsible for the name nematic [7, 10].

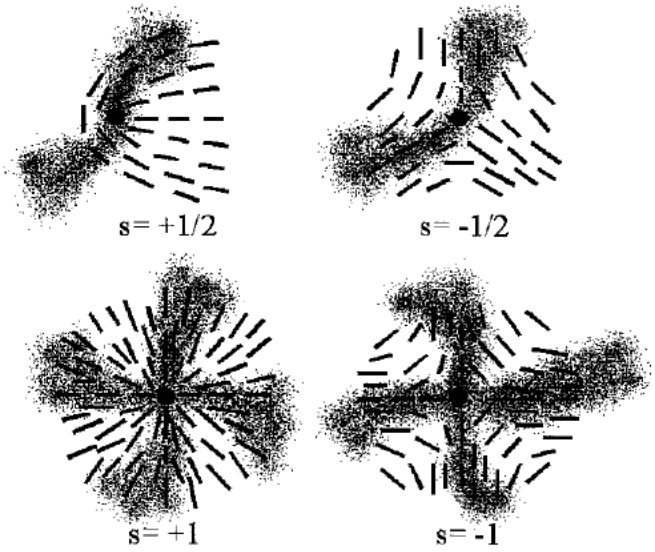

Fig. 2.4: Director configurations in the vicinity of defect lines observed in nematic Schlieren textures (from ref. [9]).

If the disclination lines make a large angle with the direction of observation they give rise to the 'threaded' texture. These disclination lines either form closed loops in the medium or end at the surfaces. In fact, these thread-like structures are responsible for the name nematic [7, 10].

2.2.1 POM Set up

A typical setup of a polarizing optical microscope is shown in figure 2.5. It consists of a light source, which is generally a halogen lamp emitting white light with a wavelength characteristic provided by the producer. The light is reflected upwards by a mirror, passes through a lens, and is linearly polarized by a polarizer, which can often be rotated by 360°. The condenser collects the light from the light source and assures a uniform illumination of the sample. For this, the aperture iris must be adjusted correctly. Additionally, the distance between the condenser and the sample has to be adjusted to focus the light beam correctly and to assure proper illumination. Microscopes for liquid crystal research are generally equipped with a rotatable stage onto which a hot stage containing the sample can be securely mounted to assure a precise rotation of the sample in a plane perpendicular to the direction of light propagation. The transmitted light then passes into the objective. This is another fundamental part of the microscope, as it crucially determines the quality of the image. After passing through the objective, the light passes through the analyzer, a second polarizer that is often rotatable by 360° and is also removable.

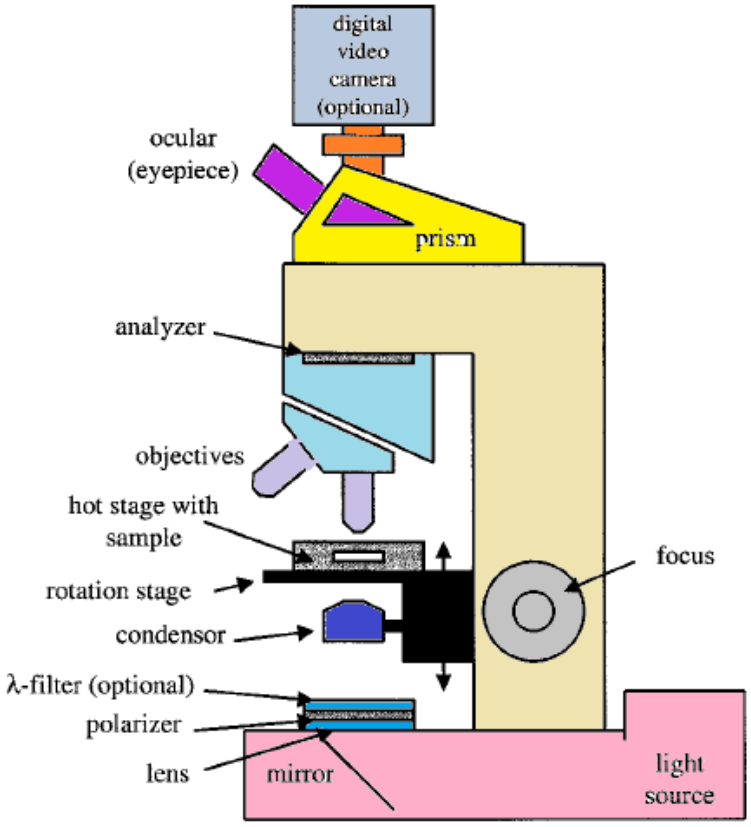

Fig. 2.5: Schematic setup of a polarizing optical microscope as used for texture studies of liquid crystalline phases (from ref. [9]).

For texture studies the analyzer is usually oriented at right angles to the polarizer, i.e. with no birefringent sample present, the field of view is black. The ocular or eyepiece serves to magnify the image further. Often a magnification of 10x is used. The ocular also determines the field of view. Alternatively, after opening a shutter or by use of a semi-transmitting mirror, the image can also be projected onto a camera mounted on the microscope.

2.3: Characterization of lyotropic liquid crystalline phases

In this section we briefly describe the characterization of some of the commonly observed lyotropic liquid crystalline phases using polarizing optical microscopy and x-ray diffraction.

2.3.1 Nematic phase

Lyotropic nematic phases is usually located between the well-ordered phases (lamellar, hexagonal) and the completely disordered (micellar solutions). The calamitic (N_c) phase is formed by rod-like micelles and occur close to the hexagonal phase. The discotic (N_d) phase is formed by disc-like micelles and occur close to the lamellar phase. In the N_c phase there is long-range correlation in

the orientation of the long axes of the rods, whereas in the N_d phase there is long-range correlation in the orientation of the normal to the discs. Under crossed polarizers, this phase exhibits, either a schlieren or thread-like texture (Fig. 2.6). In the N_d phase disc-like micelles naturally align parallel to the substrates and gives rise to large pseudo isotropic regions, on the other hand the Nc phase consisting of rodlike micelles naturally orient with their long axis parallel to the glass substrates and exhibit planer texture.

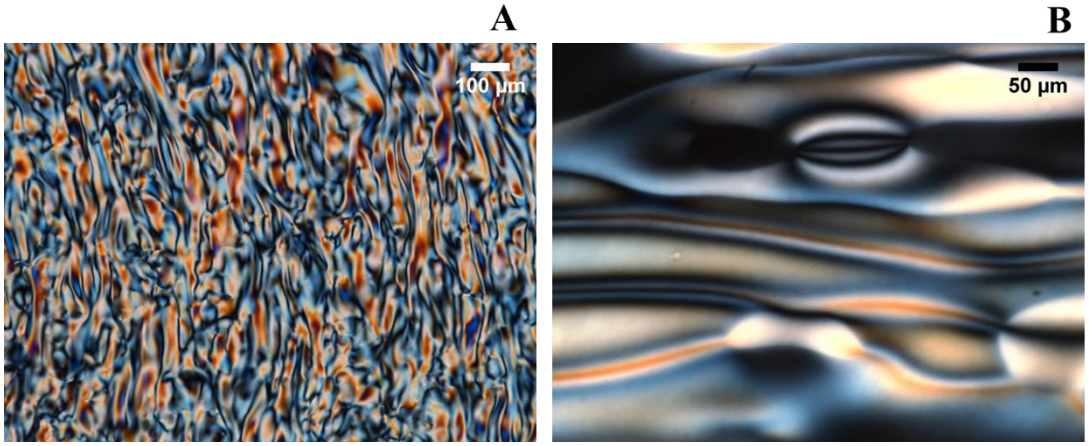

Fig. 2.6: Polarizing optical microscopy texture of nematic phase: (A) schlieren texture in the N_c phase and (B) schlieren texture along with homeotropic region in the N_d phase

When the nematic phase is subjected to homeotropic boundary conditions the director orients perpendicular to the substrates. In this case the direction of light propagation coincides with the optic axis of the phase. Rotation of the sample does not produce any change in color or intensity. This is called the pseudo-isotropic texture, because the sample appears like the isotropic phase. To distinguish between the real isotropic and the pseudo-isotropic texture of the nematic phase, one can gently press on the top glass substrate. In doing so, a bright flash will appear in the case of the nematic phase, due to mechanical reorientation of the director and therefore also the optic axis.

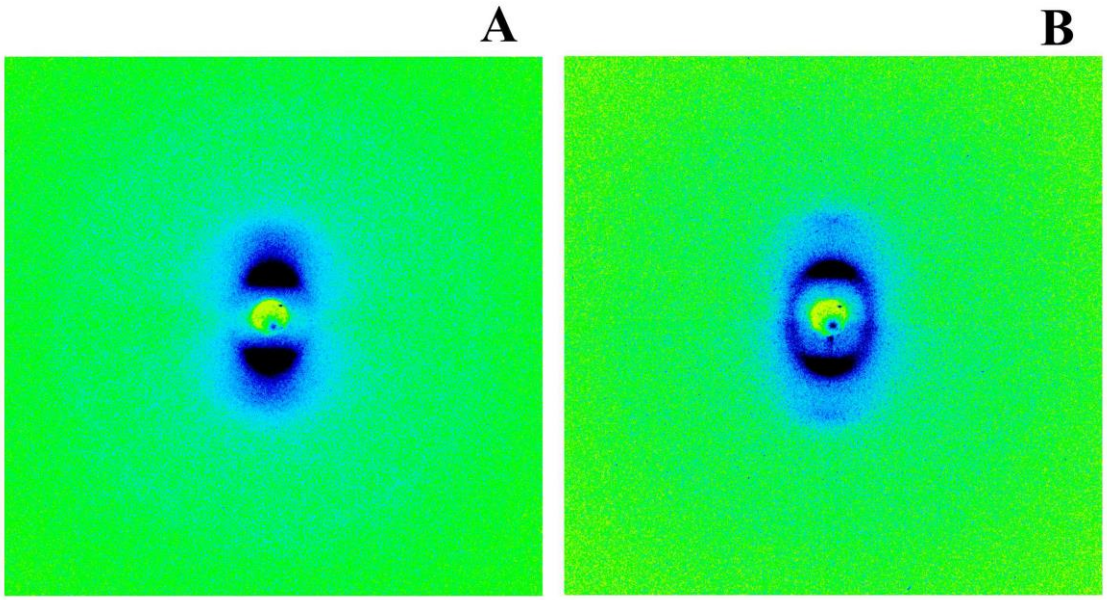

Fig.2.7: Typical diffraction pattern of nematic phases (A) N_c and (B) N_d.

There are two length scales associated with a nematic phase. One corresponds to the 'face to face' separation (d_1) of the micelles along the nematic director and other related to the 'side by side' separation (d_2) in the plane perpendicular to the director. X-ray scattering pattern of a single domain sample shows two sets of broad reflections on a 2-D detector which are perpendicular to each other and corresponding to these two length scales. These broad peaks, reflect the short-range positional order in the system. Peak related to separation d_2 in the N_c phase is sharper than the one corresponding to d_1; the d_1 peak is usually very broad in these systems due to the highly poly-disperse length distribution of the rod-like micelles. d_1 peak in N_c and d_2 peak in N_d appear in the very small angle region due the larger dimension of these aggregates along these directions. Therefore, very often, only the d_2 peak is observed from a N_c phase (along with a very diffuse peak with spacing $\frac{d_2}{\sqrt{3}}$, due to short-range hexagonal order of the rod-like micelles), and the d1 (along with a very diffuse peak with spacing $\frac{d_1}{\sqrt{1}}$, due to short-range lamellar order of the disc-like micelles) from a N_d phase. Typical diffraction patterns of the N_c and N_d phase are shown in figures 2.7 A and B, respectively.

2.3.2 Cholesteric phase

In cholesterics, the typical length scale of the pitch is of the order of micrometers. Between crossed polarizers, a film of cholesteric presents the fingerprint texture (Fig. 2.8).

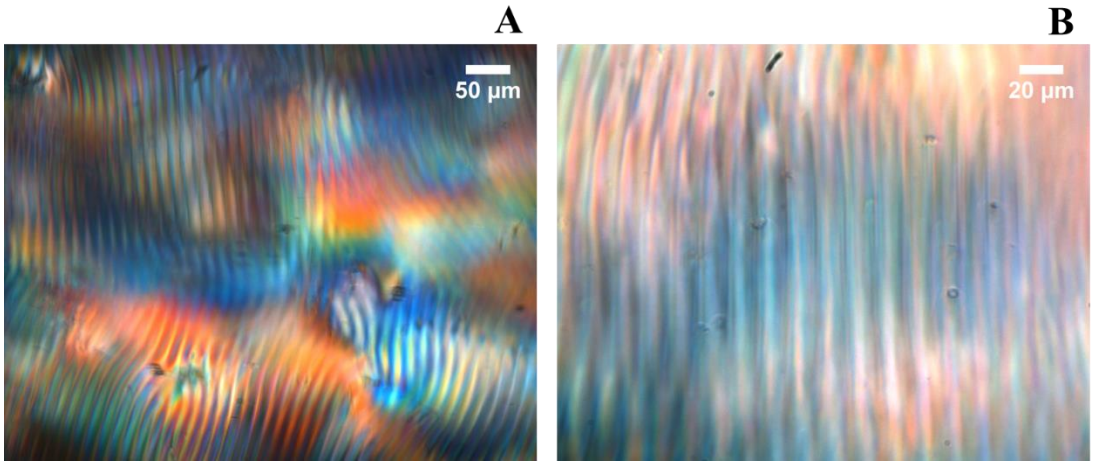

Fig. 2.8: Typical fingerprint texture of cholesteric N_c phase.

2.3.3 Hexagonal phase

This phase consists of long cylindrical aggregates arranged on a 2D hexagonal lattice. Two types of lyotropic hexagonal phases have been reported in the literature, direct (H_I) and inverted (H_{II}) hexagonal phases. The viscosity of the hexagonal phase is much larger than of the lamellar phases. Small-angle X-ray diffraction patterns of hexagonal phase present Bragg peaks, with their scattering vector (q) values in the ratios $1:\sqrt{3}:\sqrt{4}:\sqrt{7}:\ldots$, which corresponds to the (1 0), (1 1), (2 0), (2 1) ...planes of a hexagonal two-dimensional lattice (Fig. 2.9 B). At high q, the diffraction pattern shows a typical band due to the mean distance between the carbon chains (~0.5 nm). This phase shows a typical fan-like texture (Fig. 2.9 A) under a polarizing optical microscope.

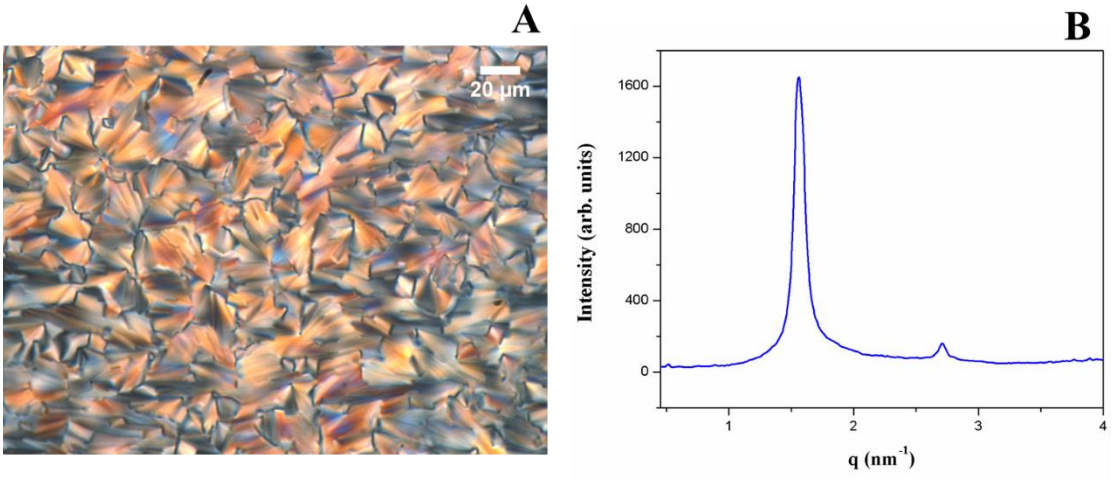

Fig. 2.9: Characterization of 2D hexagonal phase: (A) 'Fan-like texture' and (B) x-ray diffraction pattern showing two peaks with q in the ratio $1:\sqrt{3}$.

2.3.4 Lamellar phase

Lamellar phase is one of the commonly observed phases in lyotropic systems. The structural unit of the lamellar phase is the bilayer. The bilayers are stacked periodically alternating with water layers. In the fluid lamellar (L_α) phase the hydrocarbon chains of the amphiphiles are molten and the in-plane order within each bilayer is liquid-like. Like all the anisotropic phases, lamellar phases exhibit distinct optical textures, when confined in a thin slab between crossed polarizers and viewed through an optical microscope, reflecting the type of defects in the medium. Focal conics texture is often seen in the system. In the case of dilute lamellar phases, the bilayers have a strong tendency to orient parallel to the bounding surfaces, which produces a pseudo-isotropic texture with birefringent oily streaks separating the dark regions (Fig. 2.10 A). In some cases, when lamellar phase coexists with excess water, bilayers normally curl up into multilamellar vesicles and show characteristic maltese-cross texture.

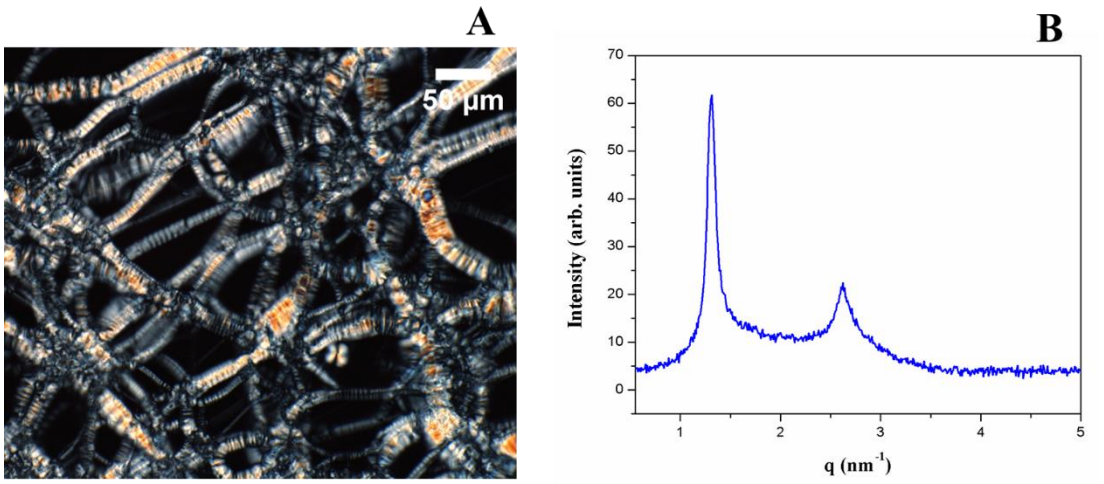

Fig. 2.10: Characterization of lamellar phase: (A) 'oily streak' texture and (B) x-ray diffraction pattern showing two peaks with q in the ratio 1:2.

Diffraction pattern of the lamellar phase consists of a set of reflections in the small angle region, with their q values in the ratio 1:2:3:4..., which is characteristic of a one-dimensional crystal (Fig. 2.10 B). L_α shows a broad peak in the wide-angle region (~0.5 nm) corresponding to the hydrocarbon chain-chain separation. The repeating distance (sum of the bilayer and water layer thickness) $d = \frac{2\pi}{q_o}$ where q_o is the position of the first peak.

2.3.5 Intermediate phases

Intermediate phases in lyotropic systems provide a topological link between the hexagonal and lamellar phases. Here we shall discuss the experimental identification of ribbon phase, random and ordered mesh phases and also of bi-continuous cubic phases.

2.3.5.1 Ribbon phase

Ribbon phases consist of long micelles with roughly elliptical cross-section, ordered on a two-dimensional rectangular lattice. This phase is birefringent. Unoriented samples of the R phase, between crossed polarizers, present a mosaic-like texture with many pseudo-isotropic regions (Fig. 2.11 A). X-ray diffraction patterns of these phases show a number of sharp peaks which can be indexed on a rectangular lattice (Fig. 2.11 B). Two types of structures have been reported, corresponding to the plane groups cmm and pgg.

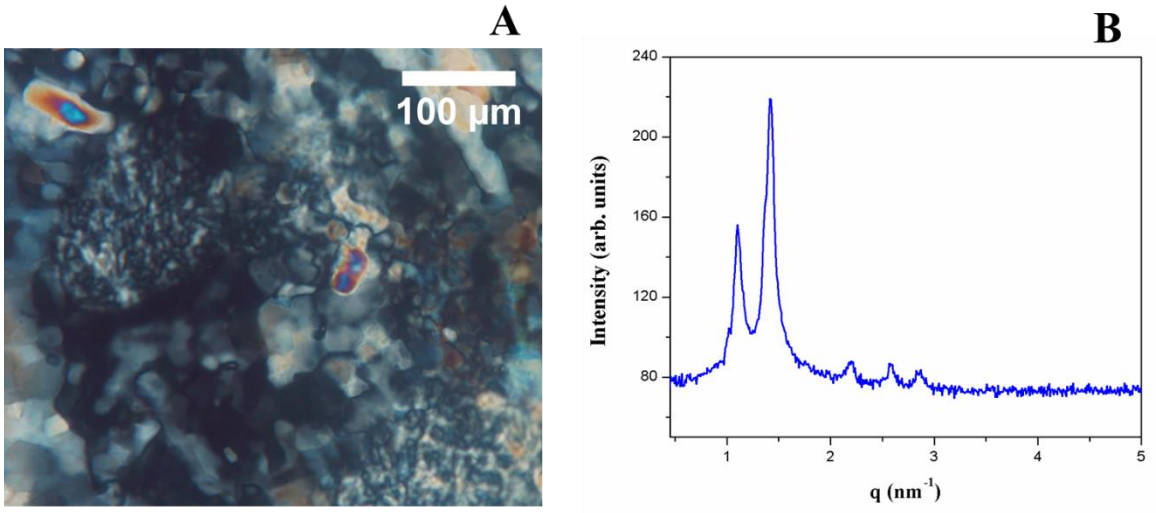

Fig. 2.11: Characterization of ribbon phase: (A) 'mosaic texture' along with 'homeotropic' region and (B) x-ray diffraction pattern showing many reflections that can be indexed on a 2D lattice of space group cmm.

2.3.5.2 Mesh phases

Mesh phases are structurally very similar to the classical lamellar phase, since they consist of stacked surfactant bilayers. However, they possess water-filled pores within the bilayers. Mesh phase is two of types; Random mesh phase and ordered mesh phase.

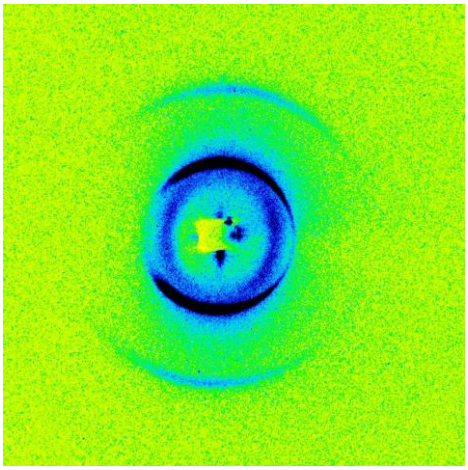

Fig. 2.12: Typical diffraction pattern of random mesh phase. The horizontal diffuse spots arise from structural inhomogeneities in the amphiphilic bilayers

In the random mesh phase, the positions of the pores are uncorrelated between and within the layers. Due to their lamellar structure, they show textures similar to those of regular lamellar phases with continuous bilayers. The random mesh phase can be distinguished from a lamellar phase consisting of regular bilayers by the presence of an additional diffuse peak in the small angle region of the X-ray diffraction pattern (Fig. 2.12). Diffraction patterns of oriented samples show that the diffuse peak occurs in a direction normal to that along which the set of peaks corresponding to the lamellar periodicity appears, indicating that the former indeed arises from in-plane inhomogeneities with short-range positional correlations.

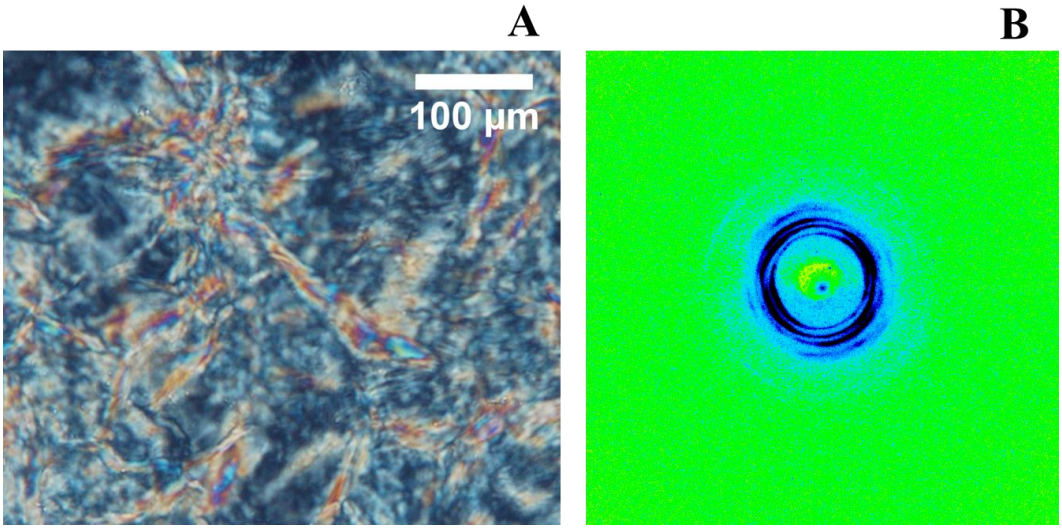

Fig. 2.13: Characterization of ordered mesh phase: (A) mosaic texture along with homeotropic region and (B) x-ray diffraction pattern showing many reflections that can be indexed on a 3D lattice of space group $R\bar{3}m$.

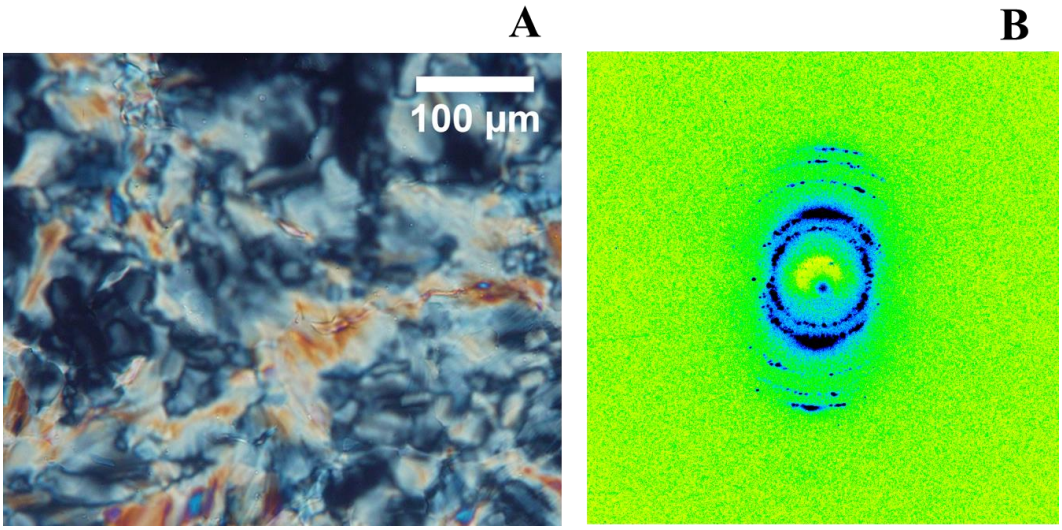

Fig. 2.14: Characterization of ordered mesh phase: (A) mosaic texture along with homeotropic region and (B) x-ray diffraction pattern showing many reflections that can be indexed on a 3D lattice of space group I4mm.

In the ordered mesh phases the mesh-like aggregates lock into a three-dimensional lattice. This phase exhibits typical mosaic texture under POM, which often contains pseudo isotropic-regions (Fig. 2.13 A and 2.14 A). This texture is quite different from that observed in random mesh phase, reflecting the change in order in the system. Diffraction pattern of the ordered mesh phase shows many reflections corresponding to the 3D structure of the system (Fig. 2.13 B and 2.14 B). Structure of the phase can be deduced from the positions of peaks by indexing it on a suitable lattice. For example, the diffraction patterns shown in figures 2.13 B and 2.14 B correspond to space groups $R\bar{3}m$ and I4mm, respectively. All known structures of ordered mesh phases are either rhombohedral (Rh) (space group: $R\bar{3}m$) or tetragonal (T) (space group: I4mm). The former consists of a 3-layer stacking of 3-coordinated hexagonal mesh, whereas the latter has a 2-layer stacking of 4-coordinated square mesh.

2.3.5.3 Cubic phase

Cubic micellar phases are not so commonly observed in lyotropic mixtures. But bi-continuous cubic phases are usually observed in narrow regions of the phase diagrams, between lamellar and hexagonal phases. Cubic phases, can be easily identified by the fact that they are optically isotropic, unlike all other phases found at comparable surfactant concentrations, which are birefringent. However, they show little flow birefringence. Diffraction patterns of these phases consist of many peaks which could be indexed on a cubic lattice and the space group symmetry of the structure can be deduced from the systematic absence of certain peaks. For example, the

diffraction pattern shown in figure 2.15 corresponds to the space group Pn3m. Cubic bi-continuous structures with space groups Ia3d, Im3m, and Pn3m have been reported in lyotropic systems.

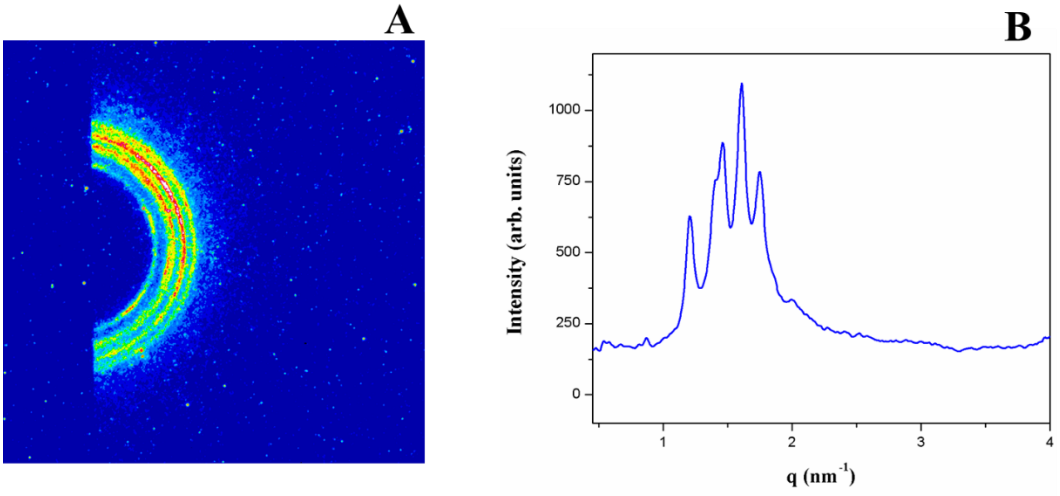

Fig. 2.15: Typical diffraction pattern of the cubic phase. X-ray diffraction pattern showing many reflections that can be indexed on a 3D lattice of space group Pn3m.

2.3.6 Sponge phase

Sponge (L_3) phase exhibits isotropic texture under polarizing optical microscopy. However, it shows flow birefringence due to flow induced alignment. The diffraction pattern of the L_3 phase, at larger q is characteristic of the scattering from randomly oriented discs. However, in the small q range, it shows a broad peak, which corresponds to a characteristic distance (Fig. 2.16), related to the average size of the cell, with short range positional ordering.

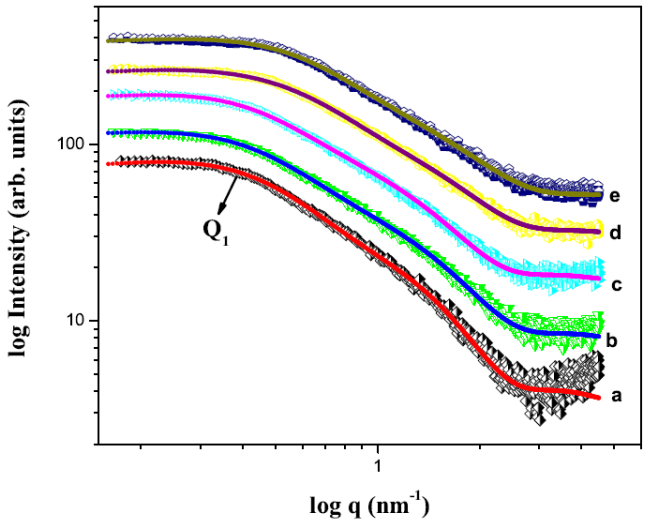

Fig. 2.16: Typical diffraction pattern of sponge phase. Q_1, the position of the broad structure peak, corresponds to the characteristic size of the cell.

References:

[1] B. E. Warren, X-ray diffraction, Dover Publications, New York (1990).

[2] D. C. Champeney, Fourier Transforms and Thier Physical Applications, Academic Press, London (1973).

[3] D. Sherwood, Crystal, X-rays and Protein, Longman, London (1976).

[4] P. J. Collings and M. Hird, Introduction to Liquid Crystals Chemistry and Physics, Taylor and Francis, Bristol (1997).

[5] G. Friedel, Ann. Phys. (Fr.), 18, 273 (1922).

[6] J. Nehring, A. Saupe, J. Chem Soc., Faraday Trans. II, 68, 1 (1972).

[7] A. Saupe, Mol. Cryst. Liq. Cryst., 21, 211 (1973).

[8] H.-R. Trebin, Adv. Phys., 31, 195 (1982).

[9] Ingo Dierking, Textures of Liquid Crystals, WILEY-VCH, Verlag GmbH & Co. KGaA, Weinheim (2003).

[10] J. Nehring, Phys. Rev. A, 7, 1737 (1973).